Free-path distribution and Knudsen-layer modeling for gaseous flows in the transition regime

Quy Dong To,[*] Céline Léonard, and Guy Lauriat

Université Paris-Est, Laboratoire Modelisation et Simulation Multi Echelle, UMR 8208 CNRS,
5 Boulevard Descartes, 77454 Marne-la-Vallée Cedex 2, France

In this paper, we use molecular dynamics (MD) simulations to study the mean free path distribution of nonequilibrium gases in micronanochannel and to model the Knudsen (Kn) layer effect. It is found that the mean free path is significantly reduced near the wall and rather insensitive to flow types (Poiseuille or Couette). The Cercignani relation between the mean free path and the viscosity is adopted to capture the velocity behavior of the special zone in the framework of the extended Navier-Stokes (NS) equations. MD simulations of flows are carried out at different Kn numbers. Results are then compared with the theoretical model.

I. INTRODUCTION

For gaseous flows in the Knudsen number (Kn) range from 0.01 to 0.1, it is possible to use the Navier-Stokes (NS) equations and slip boundary conditions at the wall. The latter concerning the linear relation between the nonzero velocity u_s and the velocity derivative $\partial u/\partial z$ can be written in the following form [1,2]:

$$u_s = \alpha\lambda \frac{\partial u}{\partial z}. \tag{1}$$

In Eq. (1) the wall is assumed to be normal to the z direction and Kn is defined as the ratio between the mean free path (MFP) λ and the characteristic length of the channel, for example, the channel height L. The parameter α is related to the accommodation coefficient σ_v as follows:

$$\alpha = \frac{2 - \sigma_v}{\sigma_v}. \tag{2}$$

One of the main causes that makes the NS equations inapplicable for higher Kn is due to the Knudsen layer. In this layer, the velocity profiles deviate significantly from the continuum solutions. The size of this zone is of the order of one mean free path (MFP) and becomes increasingly considerable for high Kn. Recently attempts in modeling fluid behaviors in this special zone through the reduced viscosity concept were presented [3–6]. The authors argued that the mean free path near the wall is not the same as in the bulk, and the viscosity, which is proportional to λ, must be modified accordingly.

Based on the molecular dynamics (MD) method, the present paper examines the mean free path profile in the channel and studies how the consideration of the variation of the MFP can do to well recover the Knudsen layer effect for the case of nonequilibrium fluids with slip boundary conditions. In contrast to previous works [5,6], the authors study the distribution of MFP in different complex situations, for example, Couette or Poiseuille flows with nondiffusive walls, which can be isotropic or anisotropic. The fluid model is of hard-sphere types from which viscosity and mean free path distribution can be recovered. In terms of Knudsen layer modeling and MFP-based viscosity, the present work does not

use a MFP distribution model but adopts MFP distribution issued from MD simulations. Regarding the velocity slip modeling, an expression based on stress and accommodation coefficients is proposed and examined directly with MD results.

II. MOLECULAR DYNAMIC SIMULATIONS

A. Pseudohard sphere potential and EMD simulation results for infinite system

To derive interatomic force in MD simulations, the pseudohard sphere potential is used with the following form [7]:

$$U(r) = 50\left(\frac{50}{49}\right)^{49}\epsilon\left[\left(\frac{\sigma}{r}\right)^{50} - \left(\frac{\sigma}{r}\right)^{49}\right] \quad \text{if} \quad r < r_c,$$

$$U(r) = 0 \quad \text{if} \quad r \geqslant r_c, \quad r_c = \frac{50}{49}\sigma. \tag{3}$$

In (3), σ and ϵ are the parameters of the potential, and together with the atomic mass m, they are used, respectively, as the reference length, energy, and mass. All the results in this work will be presented in the reduced units based on these reference quantities. It is shown that using Eq. (3), the system behaviors, e.g., the compressibility, diffusion, and structure, are very close to hard sphere fluids at moderate density and temperature [7]. Similarly at low density and high temperature limit for which the interatomic interaction are negligible, classical kinetic theory results are expected to be recovered as well. In particular, the mean free path λ_∞ and the viscosity η_∞ of fluids composed of hard spheres of diameter d at temperature T verify the expression [8,9]

$$\lambda_\infty = \frac{1}{\sqrt{2}\pi nd^2}, \quad \eta_\infty = \frac{5}{16d^2}\sqrt{\frac{k_B mT}{\pi}}, \tag{4}$$

with n being the number density and k_B the Boltzmann constant. Given the potential (3), the hard sphere diameter d is chosen equal to 1.014σ so that the MD results can best fit both relations (4)$_{1,2}$. The distribution function $f(l/\lambda_\infty)$ of the dimensionless free path l/λ_∞ follows the exponential law [10]

$$f(l/\lambda_\infty) = e^{-l/\lambda_\infty}. \tag{5}$$

Here the subscript ∞ represents quantities of an infinite system, which is different from those of confined systems

[*]quy-dong.to@u-pem.fr

studied in the later section. All these results can be found within the MD simulations of system in equilibrium (EMD). Regarding the viscosity, it can be computed by the Green-Kubo (GK) expression based on the stress autocorrelation function (SAF) [11–14]:

$$\eta_\infty = \frac{V}{k_B T} \int_0^\infty \langle \tau_{xy}(t)\tau_{xy}(0)\rangle dt. \qquad (6)$$

The instantaneous microscopic virial shear τ_{xy} is computed using the formula

$$\tau_{xy} = \frac{1}{V}\left[\sum_j m v_{jx}v_{jy} + \frac{1}{2}\sum_{i\neq j} r_{ijx}f_{ijy}\right], \qquad (7)$$

where $\boldsymbol{r}_j$ and $\boldsymbol{v}_j$ are, respectively, the position and the velocity vectors of the atom j and $\boldsymbol{f}_{ij}$ the force vector of atom j acting on atom i. For the pseudohard sphere gas at small density in consideration, the contribution of the second virial part is usually negligible in comparison with the first kinetic part (less than 1%). To accelerate the convergence of SAF integral computation, we make use of the isotropy and substitute τ_{xy} by the average of all nondiagonal elements of the pressure tensor τ_{xy}, τ_{yz}, and τ_{xz} [14].

In the EMD simulations, the gas number density is fixed at $n = 0.005\sigma^{-3}$, which corresponds to the mean free path of an infinite system in equilibrium $\lambda_\infty = 43.78\sigma$. For the free path calculation, we use the starting configuration constituted of 64 000 atoms contained in the periodic cubic box of dimension $L = 234\sigma$. The initial velocities of the atoms are assigned randomly at temperature $T = 2\epsilon/k_B$. We relax the system for 20 millions of time steps of 0.001 time unit, the time to achieve the equilibrium, after which the measurements are carried out. The free path is the distance that an atom travels between the collision events, i.e., when the distance between the two atoms is less than the distance d. To determine its distribution, the range $[0,5\lambda_\infty]$ is divided into 50 intervals, and we count the number of free paths falling within each interval. The MD results in Fig. 1 have been normalized so that the total probability is equal to 1 and showed excellent agreement with
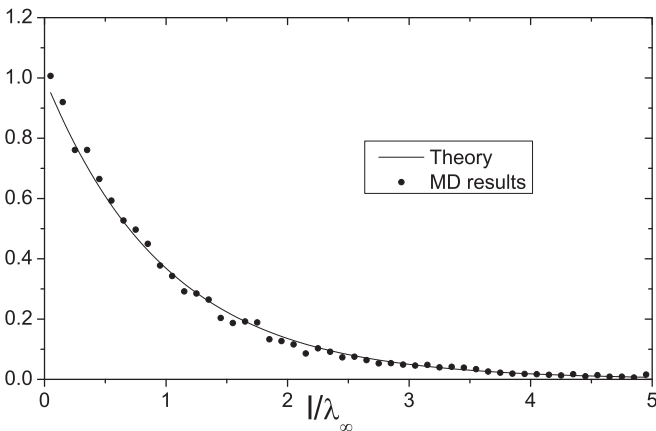

FIG. 1. Distribution function $f(l/\lambda_\infty)$ of dimensionless free path l/λ_∞. The continuous line represents the theoretical distribution $\exp(-l/\lambda_\infty)$, and the filled circles the MD results. The mean free path computed by MD simulation is 43.96σ to compared with 43.78σ from kinetic theory.
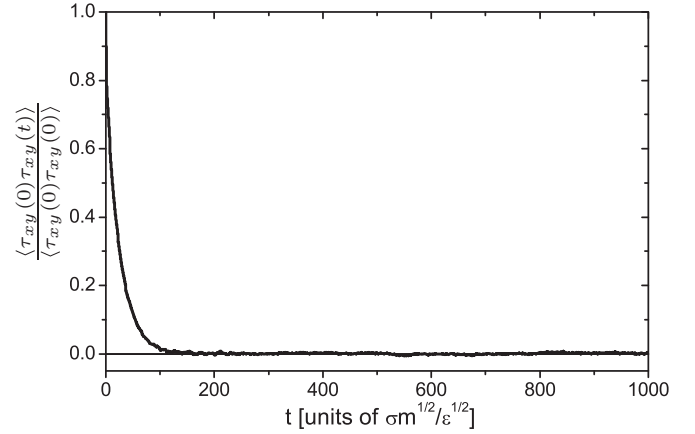

FIG. 2. Normalized SAF $\frac{\langle \tau_{xy}(0)\tau_{xy}(t)\rangle}{\langle \tau_{xy}(0)\tau_{xy}(0)\rangle}$ as function of time t (in $\sqrt{m\sigma^2/\epsilon}$ unit). The viscosity computed from the integrated SAF is 0.2539 to compared with the kinetic theory value 0.2425.

the theoretical distribution. The mean free path of the system is also very close to the theoretical value, 43.96σ by MD calculation and 43.78σ by the kinetic theory.

To calculate the viscosity using GK expression, the total integration time occurs over 1000 time units, with each time unit corresponding to an integration interval. The system is equilibrated at the same temperature using the same procedure as the previous calculation. Then the ensemble average of $\langle \tau_{xy}(t)\tau_{xy}(0)\rangle$ is taken over 30 000 samples of 64 000 atoms collected during the same run. Figure 2 shows a much longer decaying behavior of the SAF function, in comparison with Lennard-Jones (LJ) liquids. The fluctuation of the latter usually terminates at around $t = 2$ time units. For pseudohard sphere gas at the present density, due to the long collision time, the SAF function is vanishingly small after $t = 200$ time units. The viscosity integrated from SAF function yields the value $\eta_\infty = 0.2539$, which is close to value 0.2425 predicted by the kinetic theory.

All the results presented in the present section agree very well with the kinetic theory, which is valid for infinite system in equilibrium, or deviated slightly from equilibrium. In the next section, we shall investigate the case of confined nonequilibrium systems, for example, gas flow in micro- and nanochannels. In particular, we are interested in how to capture the Knudsen layer effect based on the local mean free path and viscosity.

In Ref. [6], the variation of MFP of a LJ gas in equilibrium inside a channel was considered. The authors proposed a power law to fit the variation trend of the MFP and studied the Knudsen layer effect at different Kn numbers [5]. The present paper aims at extending the approach of Ref. [6] which was based on the following discussion: (1) The LJ model was used to study Ne gas. However, the viscosity value η_∞ associated to the potential was not computed but taken elsewhere. (2) In MD simulations, the gas is in equilibrium, and the wall boundary conditions were specular reflections. (3) The empirical parameters for the power law used to fit the MFP variation were not universal enough. They may depend on the system in consideration. (4) The second order slip model was used in combination with the viscosity variation. The

coefficients were chosen to fit best the flow rate in some Kn ranges and were not linked to accommodation coefficients. Furthermore, the macroscopic agreement was only obtained at the expense of velocity profile.

As presented above in this section, the MFP and viscosity are determined uniquely from the same potential by MD calculation and agree very well with kinetic theory. In the following, we shall examine how the MFP behaves in both equilibrium and nonequilibrium conditions. Next, without assuming any wall law *a priori*, we use directly both MFP and velocity profiles obtained by MD simulations to evaluate how the approach can well reproduce the Knudsen layer.

B. Mean free path of nonequilibrium gas in confined channels

1. MFP in confined channels

In this subsection, we study gas systems with the same density $n = 0.005\sigma^{-3}$ and temperature $T = 2\epsilon/k_B$ as in the previous section. However, the periodic boundary conditions along direction z is replaced by stochastic thermal wall. Two wall models are considered: (1) Maxwell isotropic thermal wall with one accommodation parameter σ_v, (2) anisotropic thermal wall with three parameters σ_{vx}, σ_{vy}, and σ_{vz}. According to the Maxwell gas-wall collision model, σ_v is the percentage of the gas atoms that are thermalized by the wall and reflect diffusively with the temperature of the latter T_w and $1 - \sigma_v$ is the portion of atoms that reflect specularly [2]. The anisotropic wall model generalizes the Maxwell model by applying the diffusive or specular reflection mechanism to each velocity component [15]. The model is useful to capture direction-dependent effect in walls possessing two planes of symmetry, for example, atomic walls composed of infinite parallel stripes. The parameters σ_{vx}, σ_{vy}, and σ_{vz} representing the accommodation coefficients along Ox, Oy, and Oz, can be determined separately from the gas-wall collision numerical experiments [16,17]. Since the paper's scope deals with the Knudsen layer aspect, we take hypothetical values for accommodation parameters at wall temperature $T_w = 2\epsilon/k_B$ as follows:

Isotropic wall (Maxwell's model): $\sigma_v = 0.8$,

Anisotropic wall: $\sigma_{vx} = 0.96, \sigma_{vy} = 0.83$, and $\sigma_{vz} = 0.9$.

The implementation of these wall boundary conditions in MD simulations can be found in Refs. [18,19]. The number of gas atoms N and the box dimension $L_x = L_y = L_z = L$ are varied so that Kn ranges from 0.2 to 0.5 (see Table I).

The gas flows are induced by applying uniform gravity like force field (Poiseuille) $\gamma = 0.0005\epsilon/(\sigma m)$ or moving the upper wall with a constant velocity (Couette) $u_w = 0.13\sqrt{\epsilon/m}$.

TABLE I. Total number of atoms, box sizes, and Knudsen numbers of systems in consideration.

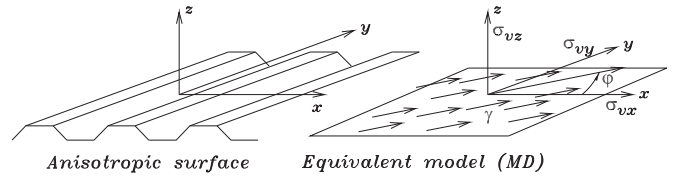| N	$L[\sigma]$	Kn $= \lambda_\infty/L$
64 000	234	0.18
27 000	178	0.25
8000	117	0.37
3375	88	0.49

FIG. 3. Model surface using directional accommodation coefficients reproducing the effects of atomic collisions on the striped surface [18,19].

along direction x. For anisotropic wall model, we define $\varphi \in [0°, 90°]$ the angle made between the force field (or wall motion) and Ox (see Fig. 3). The channels are divided into 100 layers ($N_{\text{layer}} = 100$), and we extract the mean free path, shear stress, velocity, density, and temperature profiles for each layer. Each run requires 520 millions of time steps of 0.001 time unit. The averaging process begins after achieving stabilization, i.e., 20 millions of time steps. In this work, when an atom collides with another atom or with the wall, its coordinate is recorded. When it collides again, we calculate the distance that it has traveled and update its collision coordinate, and so on. The mean free path at one layer is the average of the free paths of atoms that collide in that layer. We also distinguish average quantities associated with atoms coming from below and from above, λ_- and λ_+, and the mean free path λ for all atoms. As a result, λ_- is expected to vanish at the lower wall and to be maximal at the upper wall and vice versa. Taking atoms coming from below as an example, near the lower wall, the distance between two collisions is limited by the size of the interval $[0, z/L]$ in which the MFP is computed. But for larger values of z/L, the MPF depends mainly on the gas density. We shall compare this to an approximate analytical formula given in Ref. [20] for the layer at a distance z from the lower wall

$$\frac{\lambda_-(z)}{\lambda_\infty} = 1 + \left(\frac{z}{\lambda_\infty} - 1\right)e^{-z/\lambda_\infty} - \left(\frac{z}{\lambda_\infty}\right)^2 \text{Ei}\left(\frac{z}{\lambda_\infty}\right),$$

$$\text{Ei}(x) = \int_1^\infty \frac{e^{-xt}}{t}\,dt. \tag{8}$$

From Fig. 4 we can find that the analytical approximation of the MFP profile seems to give good results at small Kn. At higher Kn, the deviation is significant. Considering the effect of flow type (Couette or Poiseuille), we find that the mean free path is rather insensitive (see Fig. 5). Similar conclusions are obtained for different wall models (not shown): the MFP is also insensitive to the wall models and the accommodation coefficients. These remarks suggest that the distribution of MFP of quasi-isothermal and quasiuniform fluids mainly depends on the geometry and on the gas density inside the channel. We see in Fig. 6 that the variation across the channel of temperature and density obtained from MD results is almost uniform in the studied case. It can be explained by the fact that if the driving force parameters γ and u_w are small enough, the fluid deviates only slightly from equilibrium.

2. MFP-based viscosity, slip velocity

To fully capture the Knudsen layer effect, we need the slip velocity at the wall and we must know how the velocity varies into the channel center. As continuation of the previous section,
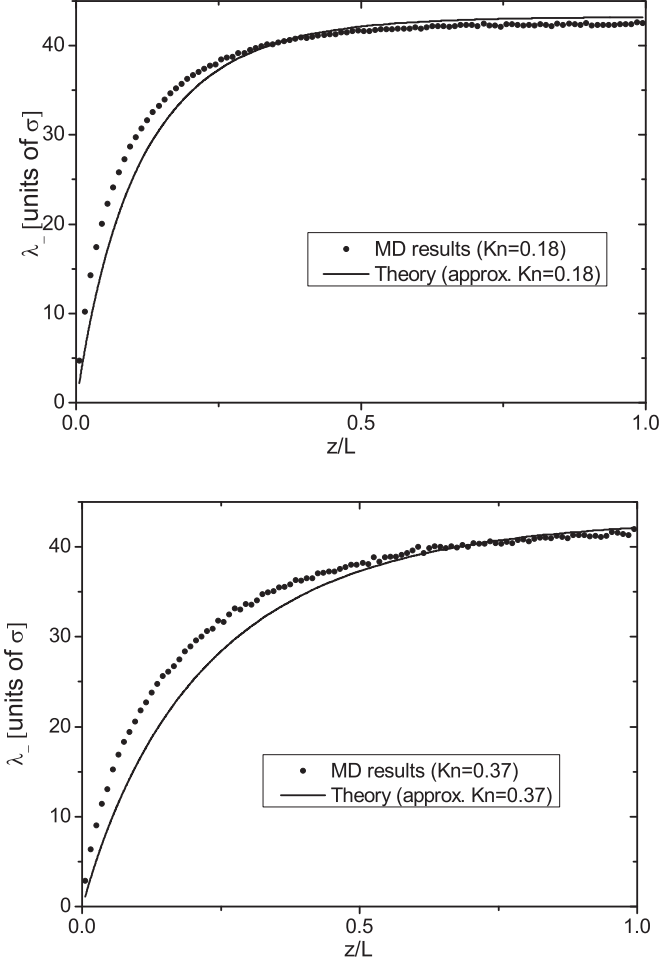
FIG. 5. (Color online) λ (in σ unit) as a function of z/L at Kn = 0.37 for Poiseuille and Couette flows. The two curves nearly superpose. The thermal wall model is the Maxwell's model with $\sigma_v = 0.8$.

FIG. 4. λ_- (in σ-unit) as function of z/L (for Kn = 0.37 and 0.18). The thermal wall model is the Maxwell's model with $\sigma_v = 0.8$.

we shall discuss first the variation of velocity profiles, which is closely related to the MFP.

Equation $(4)_2$ results from the Chapman-Enskog treatment of Boltzmann's equation [8,9], when combined with $(4)_1$, showing that the viscosity is proportional to the MFP, thermal speed and density. Such linear relation can also be derived using a less formal approach, for example, by studying the momentum transport at a control plane due to an average flux of atoms carrying the average velocity from one λ away [21,22], etc. The relation between viscosity and mean free path

$$\eta \simeq \frac{1}{2} n \bar{c} \lambda, \quad \bar{c} = \sqrt{\frac{8 k_B T}{\pi m}} \quad (9)$$

is universally accepted. However, Eq. (4) cannot explain the reduction of MFP and the velocity defect in the Knudsen layer while the density and temperature vary very slightly (see Fig. 6). A common continuum approach to deal with the Knudsen layer is to make recourse to higher order hydrodynamics models (see Refs. [1,21–24] and the references cited therein), i.e., Burnett, super Burnett, augmented Burnett, and moment equations (Grad, R13, R26), etc.

In contrast to Eq. (4), Eq. (9) is not subject to the same limitations. In recent works [3,4,6], it is suggested that one can still use the NS equation but with varying viscosity depending
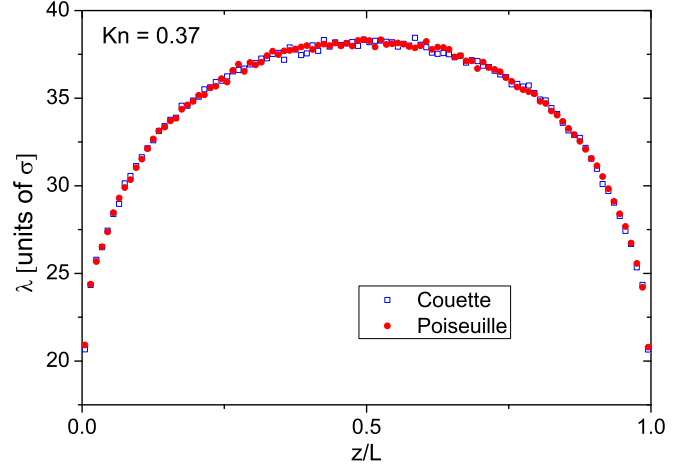
on the local mean free path $\lambda(z)$:

$$\eta(z) = \eta_\infty \frac{\lambda(z)}{\lambda_\infty}. \quad (10)$$

Here the local MFP $\lambda(z)$ is considered as given information. It can be determined accurately from MD simulations or approximated by models, as presented in the previous section.

Regarding the boundary conditions, the slip velocity $\mathbf{u}_s$ can be obtained from the accommodation coefficients. They can be written in two general forms

$$\mathbf{u}_s = \lambda \mathbf{N} \cdot \frac{\partial \mathbf{u}}{\partial z}, \quad \mathbf{u}_s = \frac{v}{m} \mathbf{N} \cdot \boldsymbol{\tau}, \quad (11)$$

where v is the collision rate at the wall and $\mathbf{N}$ is given by

$$\mathbf{N} = \begin{bmatrix} (2 - \sigma_{vx})/\sigma_{vx} & 0 \\ 0 & (2 - \sigma_{vy})/\sigma_{vy} \end{bmatrix}, \quad (12)$$
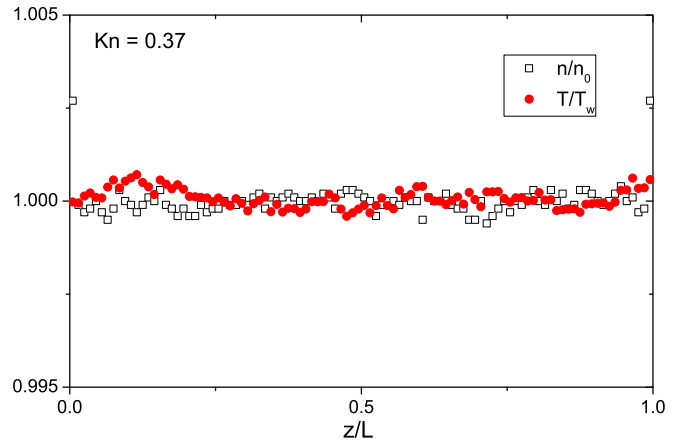

FIG. 6. (Color online) Normalized temperature T/T_w and density n/n_0 as functions of z/L at Kn = 0.37 for Poiseuille flows. The thermal wall model is the Maxwell's model with $\sigma_v = 0.8$.

in the base xOy. The derivation of Eq. (11)$_2$ is based on the association of velocity change at the wall with shear stress vector $\boldsymbol{\tau}$ via the accommodation coefficients. The two expressions (11)$_1$ and (11)$_2$ are equivalent if the NS equations are valid up to the wall and $\lambda = \lambda_\infty$. However, if these conditions are not satisfied, Eq. (11)$_1$ is subject to Knudsen layer effect and fails in the transition regime. Otherwise, we must use a correction parameter to reproduce macroscopic quantities [8,25], for example the flow rate or the macroslip. Since we focus on the variation of velocity in the Knudsen layer, Eq. (11)$_2$ will be considered. Assuming that the gas near the wall is not far from equilibrium, we can estimate the wall collision rate ν using the Maxwell Boltzmann distribution. The final equation can also be rewritten under the dimensionless form[1]

$$\frac{\boldsymbol{u}_s}{c^*} = \boldsymbol{N} \cdot \frac{\boldsymbol{\tau}}{p}, \quad c^* = \sqrt{\pi k_B T / 2m}, \qquad (13)$$

where p is the pressure. We note that when the gas-surface interaction is isotropic, i.e., $\sigma_{vx} = \sigma_{vy} = \sigma_v$, Eq. (13) is identical to Maxwell's boundary condition for isothermal flows [1,2,21]

$$\frac{u_s}{c^*} = \frac{(2 - \sigma_v)}{\sigma_v} \frac{\tau}{p}. \qquad (14)$$

3. Knudsen layer modeling and comparison with MD results

We shall continue with the previous MD experiments but now focus more on the dynamical results. First, we are looking at the shear stress profile in the channel. The local shear stress τ/p is, by definition [see Eq. (7)], computed from the product of the peculiar velocity components $\tilde{v}_{ix} = v_{ix} - u_x, \tilde{v}_{iy} = v_{iy} - u_y$, and $\tilde{v}_{iz} = v_{iz} - u_z$ along the x, y, and z directions, averaged for all atoms inside the considered bin. Here u_x, u_y, and u_z are the components of the stream velocity vector $\boldsymbol{u}$. From Fig. 7, we find that the shear stress profile is constant for Couette case and linear for Poiseuille flow. These profiles are in agreement with the solutions of the momentum conservation equation, which is universally valid. Regarding the slope of the Poiseuille case, it is also consistent with uniform body force that we apply to the fluid

$$\boldsymbol{\tau} = -nm\boldsymbol{\gamma}(z - L/2). \qquad (15)$$

The same conclusion can be obtained when the surface model is anisotropic. Since Eq. (13) can predict the slip velocity at the wall, we shall compare this value with the MD results. Table II shows that equation (13) gives a fairly accurate prediction of this quantity, i.e., around 5% difference. In order to obtain the velocity profile, the NS equations are solved considering the variation of the viscosity η associated with the variation of the mean free path [using Eq. (10)]. The velocity slope is obtained from the local Newtonian relation, for example,

$$\boldsymbol{\tau} = \eta \frac{\partial \boldsymbol{u}}{\partial z}, \qquad (16)$$

_____

[1]In works currently carried out we have used a more general approach based on a scattering kernel, the Chapman-Enskog distribution and the Grad's moment method [21] in order to model the thermal transpiration effects, the temperature jumps and velocity slip. This model reduces to Eq. (13) for the isothermal flows.
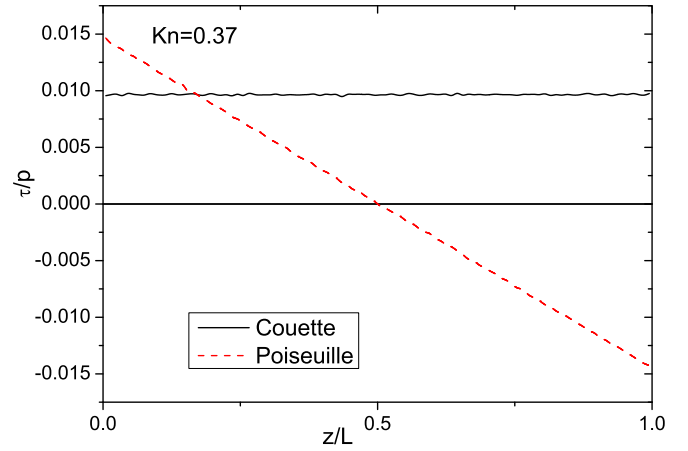

FIG. 7. (Color online) Dimensionless shear stress τ/p (vertical axis) as a function of z/L (horizontal axis) at $\mathrm{Kn} = 0.37$ for Poiseuille and Couette flows. The thermal wall model is the Maxwell's model with $\sigma_v = 0.8$.

where $\boldsymbol{\tau}$ is known by (15). Two boundary conditions are used leading to two different solutions called Approximation 1 and Approximation 2, respectively. In Approx. 1, we use the microslip at the wall. In Approx. 2, we use the MD velocity at the center of the channel. Approximation 2 is useful only to judge the quality of the viscosity approximation deduced from the velocity slope since it is meaningless in most of the modelings for which the midstream velocity is usually unknown.

To summarize, we have used the following equations to determine the velocity profile $\boldsymbol{u}$ in the interval $0 < z < L/2$ Approx. 1: Integrating Eqs. (10), (15), and (16) using slip velocity $\boldsymbol{u}(z = 0) = \boldsymbol{u}_s$ in (13) as the starting point, the mean free path function $\lambda(z)$ is calculated from MD simulations; Approx. 2: Integrating Eqs. (10), (15), and (16) using MD midstream velocity $\boldsymbol{u}(z = L/2) = \boldsymbol{u}_{MD}(z = L/2)$ as the starting point, the mean free path function $\lambda(z)$ is calculated from MD simulations.

From Fig. 8 we find that the two approximations capture very well the Knudsen layer effect demonstrated by the

TABLE II. Normalized slip velocity at the wall u_s/c^* (isotropic wall model) or slip velocity components u_{sx}/c^* and u_{sy}/c^* (anisotropic wall model, see Fig. 3) computed by MD simulations and Eq. (13). The theoretical value is calculated by Eq. (13).

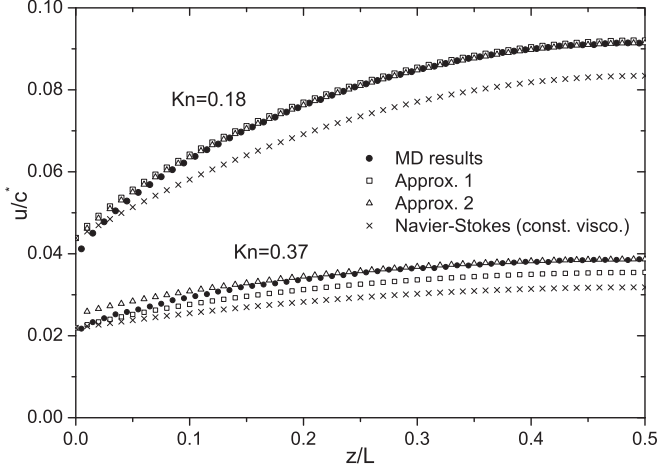| Flow/wall	Kn	φ	Dir.	MD	Theory	Diff.
Pois./Iso.	0.18	–	–	0.0410	0.0432	5%
	0.37	–	–	0.0218	0.0220	1%
	0.49	–	–	0.0173	0.0161	7%
Couette/Iso.	0.37	–	–	0.0136	0.0145	6%
Pois./Aniso.	0.18	45°	x	0.0210	0.0224	6%
			y	0.0279	0.0291	4%
	0.25	45°	x	0.0156	0.0170	8%
			y	0.0211	0.0222	5%
	0.37	45°	x	0.0109	0.0110	1%
			y	0.0149	0.0146	2%
	0.49	45°	x	0.0084	0.0084	1%
			y	0.0116	0.0110	6%

FIG. 8. Normalized velocity profile u/c^* as a function of z/L. Comparison between the MD results and the two approximations. The thermal wall model is the Maxwell's model.

disagreement between the Approx. 1 and 2 velocity profiles, and the NS solution determined from the use of constant viscosity η_∞ and slip boundary conditions, which have been defined by the microslip (13). Indeed, this disagreement is maximum at the center of the channel. The two approximations also agree well with the MD results at Kn = 0.18. At higher Kn (Kn = 0.37), Approx. 1 underestimates the velocity profiles, while Approx. 2 leads to slight overestimates. From the velocity slope, the visible difference between MD calculations, and Approx. 1 and 2 results are observed at the zone within less than a half mean free path from the wall, a zone that can be identified to a new reduced Knudsen layer. Another interesting remark can be made here that outside this Knudsen layer, the estimation of viscosity from the mean free path is particularly good at the channel center.

Since the slip velocity can be computed with relatively good accuracy from the shear stress and accommodation coefficients, we shall keep Approx. 1 in the following analysis. From Fig. 9 we can see that the approximation works well
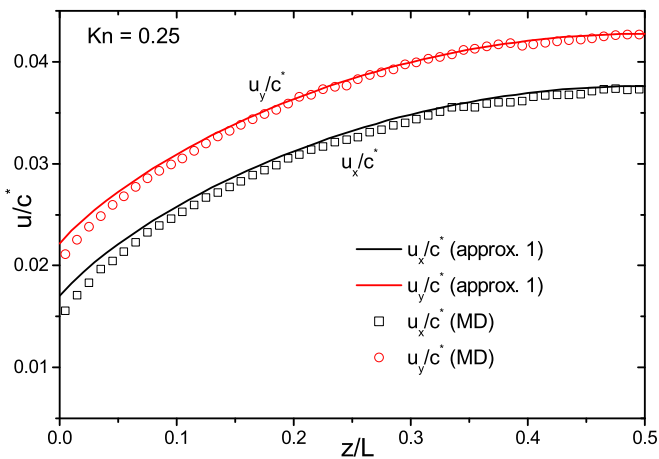

FIG. 9. (Color online) Normalized velocity components u_x/c^* and u_y/c^* as a function of z/L. Comparison between the MD results and the present approximation 1. The thermal wall model is anisotropic. The flow direction is $\varphi = 45°$.

TABLE III. Dimensionless flow rate.

Kn	$\bar{Q}_x$ (MD)	$\bar{Q}_x$ (present)	$\bar{Q}_y$ (MD)	$\bar{Q}_y$ (present)	Diff.
0.18	0.02325	0.02268	0.02662	0.02621	3%
0.25	0.01581	0.01536	0.01837	0.01808	3%
0.37	0.00911	0.00899	0.01157	0.01068	9%
0.49	0.00696	0.00626	0.00753	0.00841	12%

for flows over anisotropic surface. Generally good agreement with MD results is found for Kn = 0.25. To judge the overall performance of the approximation at different Kn, we compare the dimensionless flow rate $\bar{Q}_x$ and $\bar{Q}_y$, integrated from the normalized velocity profile

$$\bar{Q}_x = \frac{1}{2Lc^*} \int_0^L u_x \, dz, \quad \bar{Q}_y = \frac{1}{2Lc^*} \int_0^L u_y \, dz. \quad (17)$$

The results presented in Table III show that for Kn up to 0.25, the present approach agrees very well with the MD method. However, at Kn as high as 0.37, the agreement is lost. By linear interpolation, it is suggested that the method can work up to Kn = 0.3 (with 5% error).

III. CONCLUSIONS

The paper presents MD simulation results on the MFP profile of non equilibrium gas in confined channel with slip boundary conditions. This variation of the MFP profile leads to variation of the viscosity across the channel. The main results are the following.

First, the MFP strongly reduces near the wall. Second, the MFP profile is insensitive if Poiseuille or Couette flows are considered. It is also suggested that MFP is independent of the surface properties(via the influences of the accommodations coefficients and isotropy). Third, the NS equations at different Knudsen numbers have been solved for a varying viscosity, and the solutions are compared with MD solutions and NS solution with a constant viscosity. Fourth, in contrast to previous works [5,6] using empirical second-order slip coefficients for a purely diffusive wall, we have evaluated the slip velocity directly from the shear stress at the wall and accommodation coefficients which are not equal to 1 and depend on directions for anisotropic surfaces. This stress-slip velocity relation is valid for all Kn numbers under consideration. We note here that the slip velocity is the real slip velocity at the wall (microslip), not the velocity extended from the velocity profile at the center of the channel (macroslip). Finally by comparing MD results with the extended NS equations, we suggest that the latter approach works well at Kn high as 0.3 but still fails at higher Kn.

The present work approach can be extended to study different aspects. Since the stress-slip velocity relation still works while MFP based NS equations fails at high Kn (Kn ⩾ 0.4, for example), it is suggested that combining higher order dynamics model and the MFP profile can improve Knudsen layer issue at this Kn range. Further studies on its validity for different flow conditions, e.g., highly nonequilibrium fluid, complex geometry, will be done in the future. In addition, the study of the influence of accommodation coefficients with different scattering kernel models in both dynamic and heat transfer problems will also be considered.

[1] G. Karniadakis, A. Beskok, and N. Aluru, *Microflows and Nanoflows: Fundamentals and Simulation* (Springer, New York, 2005).

[2] J. Maxwell, Philos. Trans. R. Soc. A **170**, 231 (1879).

[3] M. Fichman and G. Hetsroni, Phys. Fluids **17**, 123102 (2005).

[4] Z. Guo, B. Shi, and C. Zheng, Europhys. Lett. **80**, 24001 (2007).

[5] N. Dongari, Y. Zhang, and J. M. Reese, J. Phys. D **44**, 125502 (2011).

[6] N. Dongari, Y. Zhang, and J. M. Reese, J. Fluids Eng. **133**, 071101 (2011).

[7] J. Jover, A. J. Haslam, A. Galindo, G. Jackson, and E. A. Müller, J. Chem. Phys. **137**, 144505 (2012).

[8] C. Cercignani, *Mathematical Methods in Kinetic Theory* (Plenum Press, New York, 1969).

[9] S. Chapman and T. Cowling, *The Mathematical Theory of Non-uniform Gases: An Account of the Kinetic Theory of Viscosity, Thermal Conduction, and Diffusion in Gases* (Cambridge University Press, Cambridge, 1970).

[10] E. H. Kennard, *Kinetic Theory of Gases with an Introduction to Statistical Mechanics* (McGraw-Hill, New York, 1938).

[11] D. Evans and G. Morriss, *Statistical Mechanics of Nonequilibrium Liquids* (Cambridge University Press, Cambridge, 2008).

[12] R. Kubo, J. Phys. Soc. Jpn. **12**, 570 (1957).

[13] J. Hansen and I. McDonald, *Theory of Simple Liquids* (Academic Press, New York, 2006).

[14] D. Rapaport, *The Art of Molecular Dynamics Simulation* (Cambridge University Press, Cambridge, 2004).

[15] S. Dadzie and J. Meolans, J. Math. Phys. **45**, 1804 (2004).

[16] T. T. Pham, Q. D. To, G. Lauriat, C. Léonard, and V. V. Hoang, Phys. Rev. E **86**, 051201 (2012).

[17] C. Léonard, V. Brites, T. Pham, Q.-D. To, and G. Lauriat, Eur. Phys. J. B **86**, 1 (2013).

[18] Q. D. To, T. T. Pham, V. Brites, C. Léonard, and G. Lauriat, J. Heat Transfer (to be published).

[19] T. T. Pham, Q. D. To, G. Lauriat, and C. Léonard, Phys. Rev. E **87**, 053012 (2013).

[20] D. Stops, J. Phys. D **3**, 685 (1970).

[21] H. Struchtrup, *Macroscopic Transport Equations for Rarefied Gas Flows: Approximation Methods in Kinetic Theory* (Springer, New York, 2005).

[22] W. Liou and Y. Fang, *Microfluid Mechanics* (McGraw-Hill, New York, 2006).

[23] D. A. Lockerby, J. M. Reese, and M. A. Gallis, Phys. Fluids **17**, 100609 (2005).

[24] H. Struchtrup, Continuum Mech. Therm. **17**, 43 (2005).

[25] N. G. Hadjiconstantinou, Phys. Fluids **18**, 111301 (2006).